Soil Dynamics and Earthquake Engineering 29 (2009) 1016–1026

Contents lists available at ScienceDirect

Soil Dynamics and Earthquake Engineering

journal homepage: www.elsevier.com/locate/soildyn

Direct time-domain soil profile reconstruction for one-dimensional semi-infinite domains

Seong-Won Na, Loukas F. Kallivokas *

Department of Civil, Architectural and Environmental Engineering, The University of Texas at Austin, Austin, TX 78712, USA

ARTICLE INFO

Article history:
Received 24 April 2008
Received in revised form
1 December 2008
Accepted 3 December 2008

Keywords:
Inverse medium problem
PDE-constrained optimization
Material profile reconstruction
Time-dependent regularization
Semi-infinite domains
Soil profile

ABSTRACT

We discuss the inverse medium problem associated with the reconstruction of the heterogeneous material profile of a semi-infinite (layered) soil medium, directly in the time domain, based on the complete waveform response of the medium to interrogating waves. To tackle the inversion process, we use a partial-differential-equation-constrained optimization approach, supplemented with a time-dependent regularization scheme. We introduce an absorbing boundary to truncate the semi-infinite extent of the physical domain, and propose two schemes to refine the reconstructed profiles: the first is based on iteratively re-positioning the truncation boundary until convergence, and the second is based on optimizing the observation period, so as to exclude records with information beyond the truncation boundary. We present numerical results that attest to the efficacy of the proposed schemes in reconstructing sharp profiles of semi-infinite soil domains using both noise-free and noisy data, while in the presence of absorbing boundaries.

1. Introduction

Reconstruction of material profiles for layered soils, whether in terms of elastic moduli or wave velocities, based on surficial measurements collected as the response of the soil to dynamic loads imparted on its surface is central to geotechnical site characterization efforts. The same problem, albeit at considerably different length scales, is also of primary importance to seismic hazard mitigation efforts, to soil–structure interaction problems, and to geophysics applications (e.g., discovery of hydrocarbon deposits). An often-used frequency-domain technique for geotechnical site characterization is based on the spectral-analysis-of-surface-waves (SASW) method [1]: the method relies on the analysis of surface Rayleigh waves for determining the dispersion curve that, in turn, leads to the shear wave velocity profile. The method, however, is limited in several ways, not the least of which is the assumption of a horizontally layered medium that hinders reconstruction efforts in highly heterogeneous domains in two or three spatial dimensions. The approach presented herein, though also discussed in the context of horizontally layered media, is directly extensible to heterogeneous two- and three-dimensional domains, and thus offers a viable alternative to the SASW methodology.

The approach we follow hinges on the simultaneous satisfaction of the observations (measurements), as well as of the underlying physics of the problem. To this end, our starting point is a classic misfit functional of the time-averaged difference between computed and measured response (in the least-squares sense), where the computed response refers to that calculated for a given estimate of the material profile. To enforce the satisfaction of the physics, the misfit functional is augmented via the weak imposition of the governing partial differential equations (PDEs), similar to the approach followed by Akcelik et al. [2–4], and originally suggested by Lions [5] in the 1970s. The goal is to recover the spatial distribution of the elastic modulus (or, equivalently, the wave velocity when the density is assumed constant). Overall, we are interested in recovering both smoothly varying and sharp profiles, without making an explicit distinction between the two. Within the realm of inverse problems, the problem is, naturally, tantamount to the recovery of continuous and discontinuous PDE coefficients, respectively, based on measurements. The reconstruction of discontinuous PDE coefficients, in particular, has been addressed in the numerical and inverse problem communities primarily for elliptic problems (e.g., [6]). The reconstruction of discontinuous coefficients for hyperbolic problems remains a difficult and open problem and the literature is rather thin on the subject (see though [7]). Even though we too treat the PDE coefficients as spatially smooth, as it will be seen, sharp profiles are still satisfactorily recoverable.

Once the, originally, constrained optimization problem is converted to a constrained optimization problem by means of

* Corresponding author.
E-mail addresses: swna@mail.utexas.edu (S.-W. Na), loukas@mail.utexas.edu (L.F. Kallivokas).

0267-7261/$ - see front matter © 2008 Elsevier Ltd. All rights reserved.
doi:10.1016/j.soildyn.2008.12.003

the augmented functional, we seek to enforce the functional's stationarity by requiring the vanishing of the first-order optimality conditions: upon discretization, there results a classic Karush–Kuhn–Tucker (KKT) system. Neither convexity of the augmented functional, nor worse, solution existence and/or uniqueness are guaranteed. Thus, as in most inverse problems, to narrow the solution feasibility space, it is important that specialized regularization schemes be considered. Here, we opted for a direct time-domain regularization that results in a coupled tempo-spatial formulation, which, initially, treats the design variables (distributed material parameters) as time-dependent, and enforces temporal stationarity at the end of the inversion process. We then use a reduced-space approach for the resolution of the ensuing first-order optimality conditions that result in state, adjoint, and control field problems. As will be discussed, these entail both initial, as well as final value boundary value problems. All three problems are iteratively solved until convergence of the material properties: the last obtained, spatially distributed, material property reveals the soil profile, without need for further intervention.

The time-dependent regularization scheme used herein was originally suggested by Tadi [8], where it was used for the reconstruction of the density profile of a one-dimensional elastic fixed-end rod. It was subsequently extended to the near-identical problem of the modulus inversion [9] for, again, a fixed-end rod. Recently, in [10] we compared Tadi's time-dependent scheme against two well-known spatial regularization schemes, namely, Tikhonov [11] and total variation schemes [12], for the fixed-bottom soil medium case, under inexact initial estimates, noisy data, regularization parameter choices, and for both one- and two-distributed-parameter inversions: we found its performance to be more robust than the spatial schemes, albeit at increased computational cost. Thus, here, we favor its adoption for the semi-infinite layered soil medium case we consider, where the depth-to-bottom is not *a priori* known. We remark that, from a physical perspective, the semi-infinite domain case is considerably different than the fixed-end case: in the latter case, the domain, in the absence of damping, is continuously illuminated by the wave source, whereas in the former case, the domain is only once illuminated, with the illumination lasting, roughly, as long as it is required for the wave to traverse the probed domain. The short-time illumination makes the semi-infinite case harder to invert for, than the fixed-end case.

There are also mathematical and algorithmic difficulties associated with the semi-infinite case that are not present in the fixed-end case: to tackle the semi-infinite extent of the domain, we first truncate it by imposing an absorbing boundary condition (ABC) at an arbitrarily selected truncation depth, which, in general, does not coincide with a fixed-bottom. The resulting computational domain is, in this way, rendered finite. Ideally, the ABC ought to be such that the passage of waves is ensured without any reflections from the truncation boundary, thus perfectly mimicking the physical setting. In the presence of heterogeneity, exact non-reflecting absorbing conditions are hard to devise, depend on *a priori* knowledge of the property profile at the truncation boundary, and are, typically, non-local in time. Here we opt for a local condition, which is exact only if the exterior domain is homogeneous. Therefore, since the ABC is predicated upon the assumption of homogeneity of the semi-infinite extent of the part of the medium excluded from subsequent computations (the exterior domain), the choice of the truncation location becomes critical. To this end, in this work, we contribute two schemes that guide the placement of the truncation boundary, one based on the optimal selection of the total observation time, and the other on an iterative process, whereby the truncation location is incrementally re-positioned until convergence of the reconstructed material profile.

We report numerical experiments that demonstrate robustness of the proposed time-domain scheme for inverting sharp target profiles of semi-infinite domains based on noise-free and/or noisy data, while in the presence of absorbing boundaries, and aided by the two schemes we devised for ensuring the fidelity of the reconstructed profiles. We remark that, as it will be shown, the number of layers, the elastic properties of each layer, and the layer thicknesses, are all recoverable automatically, without having to describe each layer via individual parameters, owing to the treatment of the material properties as spatially distributed.

2. Forward modeling

To fix ideas, we consider the response of a semi-infinite horizontally layered (heterogeneous) soil medium to applied stress on the top surface (Fig. 1). We formally reduce the problem to a one-dimensional one by considering, for example, the case of compressional waves emanating from the surface of the soil due to a uniform excitation applied throughout the entire (two-dimensional) soil surface. Similar physical problems arise if one were to consider only shear waves in the same medium, or compressional waves in a rod. The latter problem, as mentioned, was similarly treated by Tadi [8,9], albeit for a finite medium, without absorbing boundaries, and the schemes proposed herein. We shall henceforth refer to compressional waves, which allow the reduction of the problem to one dimension; ultimately, our target application is the three-dimensional inversion of highly heterogeneous deposits. In principle, the approach we discuss herein can be applied to this more complex problem with only minor modifications to account for the higher spatial dimensionality. Therefore, let $u(x,t)$ denote the (scalar) displacement in the direction of the applied excitation. Let T denote the total observation period. Then, the strong form of the forward problem can be stated as:

The forward problem: Find $u(x,t)$, such that

$$\partial^2 u(x,t)\partial t^2 - \frac{\partial}{\partial x}\left(\alpha(x)\frac{\partial u(x,t)}{\partial x}\right) = 0, \quad (x,t) \in (0,\infty)\times(0,T), \tag{1}$$

$$\alpha(0)\frac{\partial u}{\partial x}(0,t) = f(t), \tag{2}$$

$$\left(\frac{\partial u(x,t)}{\partial x} + \frac{1}{\sqrt{\alpha}}\frac{\partial u(x,t)}{\partial t}\right) = 0 \quad \text{for } x \geqslant \bar{x}, \tag{3}$$

$$u(x,0) = \frac{\partial u}{\partial t}(x,0) = 0, \tag{4}$$

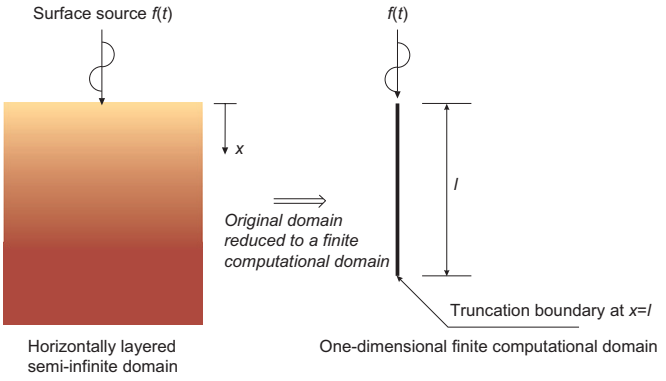

Fig. 1. Prototype 1D problem; original domain and equivalent truncated computational domain.

where x denotes location and t denotes time. In the above, $\alpha(x)$ is the soil's modulus (e.g., $\lambda+2\mu$ for compressional waves, with λ, μ denoting the Lamé constants), or the square of the wave propagation velocity. Throughout we assume that the material density is constant (a reasonable assumption in geotechnical site investigations); in particular, in (1), we assume, without loss of generality, that the density $\rho=1$. With these assumptions, (1) is the one-dimensional wave equation with a spatially varying coefficient and no damping.[1] We further assume that the system is initially at rest (condition (4)), and that the source excitation is at the origin (condition (2)). Condition (3) implies that the solution $u(x,t)$ is outgoing for some $x\geqslant\bar{x}$, where the medium becomes homogeneous, i.e., $\alpha(x)=\alpha_0$ for $x\geqslant\bar{x}$. We remark that in higher spatial dimensions, Eq. (3) is tantamount to a radiation condition.

In the inverse profile reconstruction problem, the spatial distribution of the properties $\alpha(x)$ is not known. Worse yet, $\bar{x}$ is not *a priori* known either, and the physical domain extends, on one side, to infinity. For computational purposes, we limit the semi-infinite extent by truncating the physical domain at depth $x=l$ (Fig. 1). We remark that the truncation point $x=l$ may be either greater or smaller than $\bar{x}$, that is, the exterior semi-infinite domain is either homogeneous beyond the truncation point (when $l>\bar{x}$), or heterogeneous (when $l<\bar{x}$). From a mathematical perspective, and to account for the part of the physical domain that will be left out of the computations, we introduce an absorbing boundary condition at the truncation boundary. The strong form of the resulting modified forward problem can be recast as:

Modified forward problem for truncated domain: Find $u(x,t)$, such that

$$\frac{\partial^2 u(x,t)}{\partial t^2}-\frac{\partial}{\partial x}\left(\alpha(x)\frac{\partial u(x,t)}{\partial x}\right)=0,\quad (x,t)\in(0,l)\times(0,T), \tag{5}$$

$$\alpha(0)\frac{\partial u}{\partial x}(0,t)=f(t), \tag{6}$$

$$\frac{\partial u}{\partial x}(l,t)=-\frac{1}{\sqrt{\alpha(l)}}\frac{\partial u}{\partial t}(l,t), \tag{7}$$

$$u(x,0)=\frac{\partial u}{\partial t}(x,0)=0. \tag{8}$$

We remark that for homogeneous deposits, the absorbing condition (7) is exact. For heterogeneous deposits (of interest here) it is only approximate [13], whereas the exact condition is non-local in time. From a physical point of view, the approximate character of (7) will introduce reflections at the truncation boundary, especially in the presence of strong low frequency components in the propagating waves.

3. Inverse modeling

For the physical setting described by the forward problem (5)–(8), the inverse problem can be cast as a PDE-constrained optimization problem using a (least-squares) misfit functional, as in:

Minimize:

$$\mathscr{J}=\frac{1}{2}\int_0^T[u(0,t)-u_m(0,t)]^2\,\mathrm{d}t+\mathscr{R}_\alpha(\alpha) \tag{9}$$

subject to (5)–(8).

Here, $\mathscr{J}$ is the misfit functional in which u_m denotes the response measured on the surface, and u is the computed response under an assumed modulus profile $\alpha(x)$. We seek to minimize $\mathscr{J}$, that is, to match the observation with the computed response, in an attempt to recover the spatial distribution of $\alpha(x)$, and thus to reconstruct the material profile. One primary difficulty stems from the apparent possibility of having multiple $\alpha(x)$ distributions that could yield the same surface response under the same surface excitation. Such $\alpha(x)$ distributions need not necessarily be physically meaningful. To alleviate, to an extent, such solution multiplicity, we seek to narrow the solution space by adding a regularization term $\mathscr{R}_\alpha(\alpha)$ to the misfit in (9). Two candidate schemes for $\mathscr{R}_\alpha$ are discussed in the next section.

4. Regularization schemes

One of most widely adopted regularization schemes is due to Tikhonov [11]. A Tikhonov-type regularization enforces smooth spatial variation on the model parameters (here the material profile $\alpha(x)$), and may help alleviate the inherent ill-posedness of the inverse problem. Accordingly, let $\mathscr{R}^{Tk}$ denote the regularization term per Tikhonov; $\mathscr{R}^{Tk}$ is defined as

$$\mathscr{R}^{Tk}(\alpha):=\frac{R_\alpha}{2}\int_0^l\left(\frac{\mathrm{d}\alpha}{\mathrm{d}x}\right)^2\mathrm{d}x, \tag{10}$$

where R_α is a scalar, user-defined, regularization parameter, which controls the amount by which the regularization term penalizes the misfit functional in (9). Clearly, the Tikhonov scheme favors smooth profiles, since the penalty term becomes smaller (modulo the regularization parameter) for smooth $\alpha(x)$ distributions, whereas it increases with "high-frequency" perturbations of the material parameters. Therefore, the Tikhonov scheme works well for reconstructing smooth target profiles, but is not expected to be conducive to the reconstruction of sharply varying target profiles. In addition, the Tikhonov scheme requires initial estimates that are quite close to the target, since the scheme precludes large perturbations from the initial guess. Lastly, the regularization parameter should be chosen with care, since the solution is quite sensitive to its choice [10].

An alternative choice for the regularization term is to use time-derivatives of the material parameters [8,9]. For this work, the motivation for a time-dependent scheme stems from the desire to depart from spatial regularizations that may over-penalize the spatial variability of the material parameters, often disallowing sharp material variations that are typical of soil stratifications. In this sense, as argued in [10], the only other possible dimension is to regularize the problem with respect to time, as was also done in [8,9]. We, thus, assume that $\alpha\equiv\alpha(x,t)$, that is, α becomes a function of both space and time, effectively violating the physical setting of the problem. Then, a possible form for the time-dependent regularization term $\mathscr{R}^{TD}$ is

$$\mathscr{R}^{TD}(\alpha):=\frac{R_\alpha}{2}\int_0^T\int_0^l\left(\frac{\partial\alpha(x,t)}{\partial t}\right)^2\mathrm{d}x\,\mathrm{d}t. \tag{11}$$

Even though the material parameter is assumed to depend on both time and space, at the end, the minimization process enforces it to be independent of time: of all the possible trajectories $\alpha(x,t)$ for times $t\in(0,T)$, the time-independent $\alpha(x)$ is the one minimizing (11). To this end, we further impose that

$$\alpha(x,0)=\alpha_0, \tag{12}$$

$$\frac{\partial\alpha}{\partial t}(x,T)=0. \tag{13}$$

In other words, we force at final time $t=T$, the material property distribution $\alpha(x)$ to be chosen to be the time-independent one, among all possible $\alpha(x,t)$. As will be shown numerically, this choice appears to work well for sharp profiles (in [9,10] it was shown that it

[1] In [10] we also treated the special case of viscous damping.

works well for smooth profiles as well, and it compares favorably against spatial schemes in the fixed-end problem case).

5. PDE-constrained optimization approach

5.1. Augmented functional

To reconstruct the material profile we seek to minimize (9) subject to the governing PDE and the boundary and initial conditions given by (5)–(8). To this end, we recast first the problem as an unconstrained optimization problem by defining an augmented functional based on (9) as[2]:

$$\begin{aligned}\mathscr{A}(u,\lambda,\alpha) = {} & \frac{1}{2}\int_0^T [u(0,t)-u_m(0,t)]^2\,\mathrm{d}t + \frac{R_\alpha}{2}\int_0^T\int_0^l \left(\frac{\partial\alpha}{\partial t}\right)^2 \mathrm{d}x\,\mathrm{d}t \\ & + \int_0^T\int_0^l \lambda\left\{\frac{\partial^2 u}{\partial t^2} - \frac{\partial}{\partial x}\left(\alpha\frac{\partial u}{\partial x}\right)\right\}\mathrm{d}x\,\mathrm{d}t \\ & - \int_0^T \lambda(0,t)\left\{\alpha(0,t)\frac{\partial u}{\partial x}(0,t) - f(t)\right\}\mathrm{d}t \\ & + \int_0^T \lambda(l,t)\left\{\alpha(l,t)\frac{\partial u}{\partial x}(l,t) + \sqrt{\alpha(l,t)}\frac{\partial u}{\partial t}(l,t)\right\}\mathrm{d}t \\ & + \int_0^l \lambda(x,0)\frac{\partial u}{\partial t}(x,0)\,\mathrm{d}x, \end{aligned} \tag{14}$$

where now the governing PDE and the boundary/initial conditions have been imposed (added) via Lagrange multipliers λ as side constraints. Notice that only Neumann-type conditions need to be added as part of the side constraints; any essential conditions are explicitly enforced.

5.2. The first-order optimality conditions

Next, we seek stationarity of $\mathscr{A}$ by requiring that the first-order variations of $\mathscr{A}$ with respect to the Lagrange multipliers (or adjoint variables) λ, the state variables u, and the material parameters α, vanish, or equivalently that

$$\left\{\begin{array}{c}\delta_\lambda\mathscr{A}\\ \delta_u\mathscr{A}\\ \delta_\alpha\mathscr{A}\end{array}\right\} = \mathbf{0}. \tag{15}$$

5.2.1. The first optimality condition

We require that $\delta_\lambda\mathscr{A}=0$; there results

$$\begin{aligned}\delta_\lambda\mathscr{A} = {} & \int_0^T\int_0^l \delta\lambda\left\{\frac{\partial^2 u}{\partial t^2} - \frac{\partial}{\partial x}\left(\alpha\frac{\partial u}{\partial x}\right)\right\}\mathrm{d}x\,\mathrm{d}t \\ & - \int_0^T \delta\lambda(0,t)\left[\alpha(0,t)\frac{\partial u}{\partial x}(0,t) - f(t)\right]\mathrm{d}t \\ & + \int_0^T \delta\lambda(l,t)\left\{\alpha(l,t)\frac{\partial u}{\partial x}(l,t) + \sqrt{\alpha(l,t)}\frac{\partial u}{\partial t}(l,t)\right\}\mathrm{d}t \\ & + \int_0^l \delta\lambda(x,0)\frac{\partial u}{\partial t}(x,0)\,\mathrm{d}x = 0, \end{aligned} \tag{16}$$

and by taking into account the explicitly imposed initial condition of $u(x,0)=0$, we recover the state (or forward) problem:

State problem:

$$\frac{\partial^2 u(x,t)}{\partial t^2} - \frac{\partial}{\partial x}\left(\alpha(x,t)\frac{\partial u(x,t)}{\partial x}\right) = 0, \quad (x,t)\in(0,l)\times(0,T), \tag{17}$$

$$\frac{\partial u}{\partial x}(l,t) = -\frac{1}{\sqrt{\alpha(l,t)}}\frac{\partial u}{\partial t}(l,t), \tag{18}$$

$$u(x,0) = \frac{\partial u}{\partial t}(x,0) = 0, \tag{19}$$

$$\alpha(0,t)\frac{\partial u}{\partial x}(0,t) = f(t). \tag{20}$$

5.2.2. The second optimality condition

Similarly, from the variation of the augmented functional $\mathscr{A}$ with respect to the state variable u, we obtain

$$\begin{aligned}\delta_u\mathscr{A} = {} & \int_0^T [u(0,t)-u_m(0,t)]\delta u(0,t)\,\mathrm{d}t \\ & + \int_0^T\int_0^l \lambda\left\{\frac{\partial^2\delta u}{\partial t^2} - \frac{\partial}{\partial x}\left(\alpha\frac{\partial\delta u}{\partial x}\right)\right\}\mathrm{d}x\,\mathrm{d}t \\ & - \int_0^T \lambda(0,t)\alpha(0,t)\frac{\partial\delta u}{\partial x}(0,t)\,\mathrm{d}t \\ & + \int_0^T \lambda(l,t)\left\{\alpha(l,t)\frac{\partial\delta u}{\partial x}(l,t) + \sqrt{\alpha(l,t)}\frac{\partial\delta u}{\partial t}(l,t)\right\}\mathrm{d}t \\ & + \int_0^l \lambda(x,0)\frac{\partial\delta u}{\partial t}(x,0)\,\mathrm{d}x. \end{aligned} \tag{21}$$

Integrating by parts, while taking into account any homogeneous essential boundary and initial conditions, there results

$$\begin{aligned}\delta_u\mathscr{A} = {} & \int_0^T\int_0^l \delta u\left\{\frac{\partial^2\lambda}{\partial t^2} - \frac{\partial}{\partial x}\left(\alpha\frac{\partial\lambda}{\partial x}\right)\right\}\mathrm{d}x\,\mathrm{d}t \\ & + \int_0^T \delta u(0,t)\left\{[u(0,t)-u_m(0,t)] - \alpha(0,t)\frac{\partial\lambda}{\partial x}(0,t)\right\}\mathrm{d}t \\ & + \int_0^T \delta u(l,t)\left\{\alpha(l,t)\frac{\partial\lambda}{\partial x}(l,t) - \frac{\partial}{\partial t}(\sqrt{\alpha(l,t)}\lambda(l,t))\right\}\mathrm{d}t \\ & + \int_0^l \lambda(x,T)\frac{\partial\delta u}{\partial t}(x,T)\,\mathrm{d}x + \lambda(l,T)\sqrt{\alpha(l,T)}\delta u(l,T) \\ & - \int_0^l \frac{\partial\lambda}{\partial t}(x,T)\delta u(x,T)\,\mathrm{d}x. \end{aligned} \tag{22}$$

Since δu is arbitrary, by setting $\delta_u\mathscr{A}=0$ we obtain the following adjoint problem:

Adjoint problem:

$$\frac{\partial^2\lambda(x,t)}{\partial t^2} - \frac{\partial}{\partial x}\left(\alpha(x,t)\frac{\partial\lambda(x,t)}{\partial x}\right) = 0, \quad (x,t)\in(0,l)\times(0,T), \tag{23}$$

$$\alpha(l,t)\frac{\partial\lambda}{\partial x}(l,t) = \frac{\partial}{\partial t}(\sqrt{\alpha(l,t)}\lambda(l,t)), \tag{24}$$

$$\lambda(x,T) = \frac{\partial\lambda}{\partial t}(x,T) = 0, \tag{25}$$

$$\alpha(0,t)\frac{\partial\lambda}{\partial x}(0,t) = [u(0,t)-u_m(0,t)]. \tag{26}$$

Notice that the governing operator in the adjoint PDE (23) is identical to that of the state problem (17). In addition, the absorbing boundary condition has changed sign, and from a temporal point of view, the problem has reversed direction, that is, it is a final value problem, as betrayed by (25), as opposed to an initial value problem. Lastly, notice that, by virtue of (26), the adjoint problem is driven by the misfit between computed and observed responses. From an implementation point of view, the fact that both the state and adjoint problems share the same governing operator can be exploited to reduce the computational cost. However, the storing of the time histories for both u and λ is

[2] We assume that $\alpha=\alpha(x,t)$ to pave the path for the time-dependent regularization; the case of Tikhonov regularization is simpler and can be similarly treated.

unavoidable, given the simultaneous, but in opposite direction, traversing of the time line.

5.2.3. The third optimality condition

Lastly, the variation of the augmented functional with respect to α yields

$$\delta_\alpha \mathscr{A} = R_\alpha \int_0^T \int_0^l \frac{\partial \alpha}{\partial t}\frac{\partial \delta\alpha}{\partial t}\,\mathrm{d}x\,\mathrm{d}t - \int_0^T \int_0^l \lambda \frac{\partial}{\partial x}\left(\delta\alpha \frac{\partial u}{\partial x}\right)\mathrm{d}x\,\mathrm{d}t - \int_0^T \lambda(0,t)\delta\alpha(0,t)\frac{\partial u}{\partial x}(0,t)\,\mathrm{d}t + \int_0^T \lambda(l,t)\left\{\delta\alpha(l,t)\frac{\partial u}{\partial x}(l,t) + \frac{\delta\alpha(l,t)}{2\sqrt{\alpha(l,t)}}\frac{\partial u}{\partial t}(l,t)\right\}\mathrm{d}t. \quad (27)$$

By integrating by parts, and taking into account that $(\partial\alpha/\partial t)(x,T) = 0$ and $\delta\alpha(x,0) = 0$, while canceling like-terms, (27) yields the *control problem* for α as

Control problem:

$$\delta_\alpha \mathscr{A} = \int_0^T \int_0^l \left\{ - R_\alpha \frac{\partial^2 \alpha(x,t)}{\partial t^2} + \frac{\partial \lambda(x,t)}{\partial x}\frac{\partial u(x,t)}{\partial x} + \frac{\lambda(x,t)}{2\sqrt{\alpha(x,t)}}\frac{\partial u(x,t)}{\partial t}\Delta(x-l)\right\}\delta\alpha(x,t)\mathrm{d}x\,\mathrm{d}t = 0, \quad (28)$$

where $\Delta(x-l)$ denotes the Dirac delta function.

6. The inversion process

Seeking a solution for the triad (u,λ,α) that simultaneously satisfies all three optimality conditions is tantamount to the stationarity of the augmented functional $\mathscr{A}$, and therefore to a distribution of the material properties $\alpha(x)$ that respects the observations. In principle, the state (17)–(20), the adjoint (23)–(26), and the control problem (28) can be solved as a fully coupled problem, i.e., by using a full-space method. However, the computational cost per (material property) iteration increases, given the resulting matrix sizes. We remark that for the solution of the state and the adjoint problems (either as a coupled system or individually) any numerical scheme may be used (finite differences, finite elements, etc.). By contrast to a full-space method, here we opt for a reduced-space method that maps the optimization problem to the space of the design variables (α), thereby eliminating the state and adjoint variables. We start by solving the state problem (17)–(20) to obtain the state variables u, for given estimates of the material parameters α, thereby satisfying the first optimality condition $\delta_\lambda \mathscr{A} = 0$. Then, we solve the adjoint problem using the state variables computed in the first step, to obtain the Lagrange multipliers λ that satisfy the second optimality condition $\delta_u \mathscr{A} = 0$. To solve both the state and adjoint problems, we employ conventional finite elements. Again, owing to the self-adjoint operator of the original problem, the system matrices of both the state and adjoint problems are identical. Then, there remains to seek to update the material parameters α so that the third condition (28) be satisfied. We use the control equation to iteratively provide updates to the material parameters. The details of the inversion process follows.

6.1. State and adjoint semi-discrete forms

In order to satisfy the first KKT system for assumed inversion material parameters α, we solve the state problem given in (17)–(20) using a standard Galerkin approach. Accordingly, the weak form can be obtained by multiplying the state equation (17) by an appropriate test function $\upsilon(x)$ (with $\upsilon(l) = 0$) and integrating over the entire domain. Using integration by parts, there results

$$\int_0^l \left[\frac{\partial^2 u(x,t)}{\partial t^2}\upsilon(x) + \alpha(x,t)\frac{\partial u(x,t)}{\partial x}\frac{\mathrm{d}\upsilon(x)}{\mathrm{d}x}\right]\mathrm{d}x + \upsilon(l)\sqrt{\alpha(l,t)}\,\frac{\partial u}{\partial t}(l,t) = -\upsilon(0)f(t), \quad (29)$$

where the boundary conditions have been taken into account. With a similar process, where $q(x)$ is now used as a test function, we obtain the weak form of the adjoint problem:

$$\int_0^l \left[\frac{\partial^2 \lambda(x,t)}{\partial t^2}q(x) + \alpha(x,t)\frac{\partial \lambda(x,t)}{\partial x}\frac{\mathrm{d}q(x)}{\mathrm{d}x}\right]\mathrm{d}x - q(l)\sqrt{\alpha(l,t)}\frac{\partial \lambda(l,t)}{\partial t} = q(0)[u_m(0,t) - u(0,t)]. \quad (30)$$

Next, we introduce standard polynomial approximations for the state $u(x,t)$, the adjoint $\lambda(x,t)$, and their respective test functions $\upsilon(x)$, and $q(x)$; let

$$u(x,t) = \sum_{i=1}^N u_i(t)\phi_i(x), \quad \upsilon(x) = \sum_{i=1}^N \upsilon_i\phi_i(x), \quad (31)$$

$$\lambda(x,t) = \sum_{i=1}^N \lambda_i(t)\phi_i(x), \quad q(x) = \sum_{i=1}^N q_i\phi_i(x), \quad (32)$$

where N is the number of nodal points, ϕ are basis functions, and $u_i, \lambda_i, \upsilon_i, q_i$ denote nodal quantities. Then, the semi-discrete forms of the state and adjoint problems can be cast as

$$\boldsymbol{M}\,\frac{\partial^2 \boldsymbol{u}(t)}{\partial t^2} + \boldsymbol{K}(t)\,\boldsymbol{u}(t) + \boldsymbol{C}(t)\,\frac{\partial \boldsymbol{u}(t)}{\partial t} = \boldsymbol{F}(t), \quad (33)$$

$$\boldsymbol{M}\frac{\partial^2 \boldsymbol{\lambda}(t)}{\partial t^2} + \boldsymbol{K}(t)\boldsymbol{\lambda}(t) - \boldsymbol{C}(t)\,\frac{\partial \boldsymbol{\lambda}(t)}{\partial t} = \boldsymbol{G}(t), \quad (34)$$

where

$$M_{ij} = \int_0^l \phi_i\phi_j\,\mathrm{d}x, \quad (35)$$

$$K_{ij}(t) = \int_0^l \alpha(x,t)\frac{\mathrm{d}\phi_i}{\mathrm{d}x}\frac{\mathrm{d}\phi_j}{\mathrm{d}x}\,\mathrm{d}x, \quad (36)$$

$$C_{ij}(t) = \sqrt{\alpha(l,t)}\delta_{iN}\delta_{jN}, \quad (37)$$

$$F_i = -f(t)\delta_{i1}, \quad (38)$$

$$G_i = [u_m(0,t) - u(0,t)]\delta_{i1}. \quad (39)$$

In the above, δ_{i1} and δ_{iN} denote the Kronecker delta, $\boldsymbol{u}$ and $\boldsymbol{\lambda}$ are the vectors of the nodal state and adjoint variables, respectively, and customary notation has been used for the matrices. Notice that because of the time-dependent regularization scheme, where the material distribution is assumed to be time-dependent, the mass matrix $\boldsymbol{M}$ is independent of time, but the stiffness $\boldsymbol{K}$ and damping $\boldsymbol{C}$ matrices depend on time.

6.2. Temporal discretization

To arrive at a solution, first for the state variables, and then for the adjoint variables, the semi-discrete forms (33) and (34) need next be discretized in time. We note that, whereas (33) is an initial value problem for which $\boldsymbol{u}(0) = (\partial\boldsymbol{u}/\partial t)(0) = \boldsymbol{0}$, (34) is a final value problem for which $\boldsymbol{\lambda}(T) = (\partial\boldsymbol{\lambda}/\partial t)(T) = \boldsymbol{0}$. In addition, the time-dependent matrices $\boldsymbol{K}(t)$ and $\boldsymbol{C}(t)$ need to be appropriately treated. Their temporal dependence stems from the moduli, which in turn, need also be discretized in both space

and time. Accordingly, let

$$\alpha(x,t)=\sum_{j=1}^{N} a_j(t)\varphi_j(x), \tag{40}$$

in which φ_j are basis functions, and a_j denotes nodal values of α. At the first iteration we start with a spatial distribution of the modulus $\alpha(x)$ (i.e., we enforce, initially, the modulus to be constant in time). Upon updating the modulus, there will result a spatially variable and time-dependent modulus $\alpha(x,t)$. Next, using the latter update, one could formally proceed by also updating $\boldsymbol{K}(t)$, and $\boldsymbol{C}(t)$, per (36) and (37). However, such an approach is computationally costly, as it entails the evaluation of, primarily, the stiffness matrix, on a per time-step basis. Alternatively, one could approximate the temporal dependence of the moduli by constant values (per inversion iteration); candidate choices include

$$a_j(t)\simeq\langle a_j(t)\rangle \quad \text{or} \quad a_j(t)\simeq a_j(T), \quad \forall j=1,\ldots,N, \tag{41}$$

where the former expression refers to the mean value of $a_j(t)$ over the period $(0,T)$, and the latter expression refers to its final value (similarly, for the coefficients of β, b_j). We opted for the second of (41) (piecewise constant in space, as well). Thus, effectively, over an element e, (40) can be rewritten as

$$\alpha(x,t)|_e\simeq a_e(T). \tag{42}$$

Consequently, the element matrix $\boldsymbol{k}_e$, and $\boldsymbol{c}_e$, corresponding to $\boldsymbol{K}$ and $\boldsymbol{C}$ in (36) and (37), respectively, are modified to now read

$$\boldsymbol{k}_e=a_e(T)\int_e \frac{\partial\boldsymbol{\phi}}{\partial x}\frac{\partial\boldsymbol{\phi}^{\mathrm{T}}}{\partial x}\,\mathrm{d}x, \quad \boldsymbol{c}_e=\sqrt{a_e(T)}\delta_{eN}. \tag{43}$$

A variant of the latter scheme was used in [8], whereas in [10] we showed that only minor differences are observed in the numerical results between the two schemes. Here, we used the simpler and less costly second scheme. Next, standard time integration schemes can be used: we opted for Newmark's average-acceleration scheme. We remark that the effective stiffness matrix implicated in the Newmark scheme ($\hat{\boldsymbol{K}}=\boldsymbol{K}+(4/\Delta t^2)\boldsymbol{M}+(2/\Delta t)\boldsymbol{C}$) is the same for both the state and the adjoint problems, and thus it needs to be inverted (or triangularized) only once.

6.3. Material parameter updates

By solving the state and adjoint problem, the state variable u and the adjoint variable λ satisfying the first and the second optimality conditions, respectively, are obtained. Then, the problem is reduced to a minimization problem with respect to the material parameters α. Here, notice that the variation of the augmented functional with respect to the material parameter α, $\delta_\alpha\mathscr{A}$, is tantamount to the gradient component of the misfit functional, $\nabla_\alpha\mathscr{J}$, since the side constraints in the augmented functional (14) have already vanished owing to the satisfaction/solution of the state problem. Then, what remains to be done is to provide a mechanism for updating the material parameters: this can be directly accomplished via the control equation given in (28). We outline the details below: (28) yields

$$\frac{\partial^2\alpha(x,t)}{\partial t^2}=\frac{1}{R_\alpha}\left\{\frac{\partial\lambda(x,t)}{\partial x}\frac{\partial u(x,t)}{\partial x}+\frac{\lambda(x,t)}{2\sqrt{\alpha(x,t)}}\frac{\partial u(x,t)}{\partial t}\Delta(x-l)\right\}. \tag{44}$$

The right-hand-side of (44) can be readily computed, once u and λ have been obtained. Then, the update to α can be obtained using (44), and the approximations (31) and (32), by integrating (44) twice in time, while taking into account the conditions shown below (superscripts to a indicate new and previous values between inversion iterations):

$$\begin{aligned}\alpha_e^{(k+1)}=a_e^{(k)}(t)=a_e^{(k)}(T)-\frac{t}{R_\alpha}\int_0^{\mathrm{T}}\Bigg\{&\frac{\mathrm{d}\boldsymbol{\phi}^{\mathrm{T}}}{\mathrm{d}x}\boldsymbol{\lambda}(\tau)\frac{\mathrm{d}\boldsymbol{\phi}^{\mathrm{T}}}{\mathrm{d}x}\boldsymbol{u}(\tau)\\&+\frac{1}{2\sqrt{\alpha(x,\tau)}}\boldsymbol{\phi}^{\mathrm{T}}(x)\boldsymbol{\lambda}(\tau)\boldsymbol{\phi}^{\mathrm{T}}(x)\frac{\mathrm{d}\boldsymbol{u}(\tau)}{\mathrm{d}\tau}\Delta(x-l)\Bigg\}\mathrm{d}\tau\\&+\frac{1}{R_\alpha}\int_0^t\int_0^s\Bigg\{\frac{\mathrm{d}\boldsymbol{\phi}^{\mathrm{T}}}{\mathrm{d}x}\boldsymbol{\lambda}(\tau)\frac{\mathrm{d}\boldsymbol{\phi}^{\mathrm{T}}}{\mathrm{d}x}\boldsymbol{u}(\tau)\\&+\frac{1}{2\sqrt{\alpha(x,\tau)}}\boldsymbol{\phi}^{\mathrm{T}}(x)\boldsymbol{\lambda}(\tau)\boldsymbol{\phi}^{\mathrm{T}}(x)\frac{\mathrm{d}\boldsymbol{u}(\tau)}{\mathrm{d}\tau}\Delta(x-l)\Bigg\}\mathrm{d}\tau\,\mathrm{d}s,\end{aligned} \tag{45}$$

where $\boldsymbol{\phi}$, $\boldsymbol{\lambda}$, and $\boldsymbol{u}$ are restricted to element e, and we have enforced

$$a_e^{(k+1)}(0)=a^{(k)}(T), \quad \frac{\partial a_e^{(k+1)}}{\partial t}(T)=0. \tag{46}$$

We remark that, whereas the regularization parameter R_α can be chosen arbitrarily to equal a fixed value at the onset of the inversion process, an alternative approach, based on an inexact line search scheme, leads to an optimal choice for the regularization parameter. Specifically, in (45), the integrals play the role of the search direction and the reciprocal of the regularization parameter plays the role of the step length. Therefore, by combining any gradient-based scheme with a line search, we could obtain an optimal value for the regularization parameter, and, thus, accelerate the convergence rate. To this end, we use steepest descent with an inexact line search scheme; the process is summarized in Algorithm 1.

Algorithm 1 Inversion algorithm using time-dependent regularization with optimal regularization factor

```
Choose θ, ρ, μ, R_α
Set k = 0
Set initial guess of inversion variables, a_e^k
Set convergence tolerance TOL
Set misfit = TOL + 1
while (misfit > TOL) do
  Solve the state problem (17)–(20) and obtain u
  Solve the adjoint problem (23)–(26) and obtain λ
  Compute ∂²α^(k)/∂t² using:
  d²a_e^(k)/dt² = 1/(R_α ∂x ∂x)|_e + 1/(R_α 2√α ∂t) λ ∂u Δ(x − l)
  Compute the search direction d^(k)(t), where
  d^(k)(t) = −t ∫_0^T ∂²a^(k)(τ)/∂τ² dτ + ∫_0^t ∫_0^s ∂²a^(k)(τ)/∂τ² dτ ds,
  while (J(a^(k) + θ^(k) d^(k)) > J(a^(k)) + μθ^(k) a^(k) · ∇J(a^(k))) do
    θ ← ρθ
  end while
  Update the estimates a^(k+1) = a^(k) + θ^(k) d^(k)
  k = k + 1
endwhile
```

7. Optimal positioning of the truncation boundary

Thus far we have described the inversion process by which we could reconstruct the heterogeneous material profile of a horizontally layered medium when the lack of *a priori* information on the depth-to-bottom necessitates the introduction of a truncation boundary and its associated ABC. However, as discussed earlier, the ABC is predicated upon the assumption of a homogeneous medium past the truncation boundary. In general, at a given site, the presence of homogeneity beyond a certain depth cannot be guaranteed. But even if there is a depth beyond which material homogeneity can be safely assumed, that depth,

which would have been the ideal location for truncating the physical domain, is not *a priori* known. To address the difficulty with the selection of an appropriate depth for truncating the physical domain, we introduce two schemes, both iterative in nature.

Scheme 1. *Iterative relocation of the truncation boundary.*

We assume that there is a depth beyond which the medium is indeed homogeneous, and seek to place the truncation boundary at the bottom of the very layer where the homogeneity begins (or beyond). Our iterative process is as follows: (a) first, we truncate the domain at an arbitrary depth $x = x^{(0)}$, and invert to obtain the material profile; (b) next, we increase the domain depth and truncate at $x = x^{(1)}$, where $x^{(1)} > x^{(0)}$, and invert again to obtain a new material profile; (c) we compare the profiles from steps (a) and (b) (up to $x^{(0)}$), and if the difference is small (in an appropriate norm), we consider the process converged; otherwise, we increase again the domain depth to $x^{(2)}$, with $x^{(2)} > x^{(1)}$ and obtain anew the material profile. We repeat steps (b) and (c) until convergence.

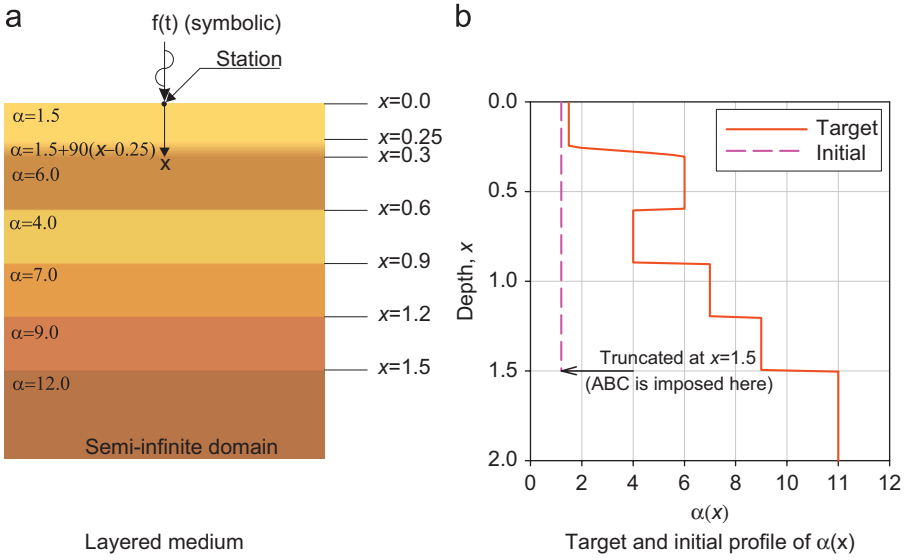

Fig. 2. Problem configuration. (a) Layered medium and (b) target and initial profiles of $\alpha(x)$.

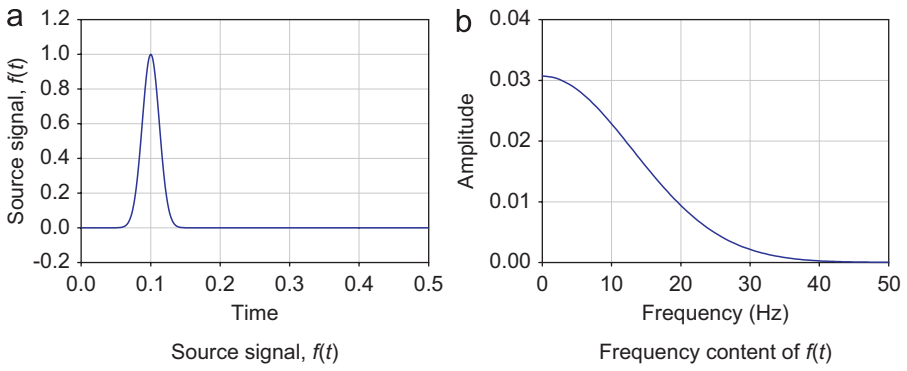

Fig. 3. Source signal, $f(t)$ (a) and its frequency transform (b).

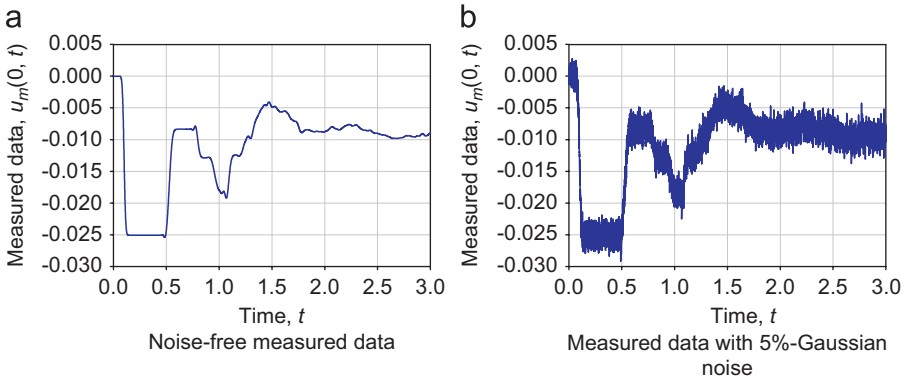

Fig. 4. Measured data, $u_m(0,t)$. (a) Noise-free measured data and (b) measured data with 5%-Gaussian noise.

Through this iterative scheme, we can typically position the truncation boundary within the homogeneous semi-infinite extent of the domain. However, in the absence of a homogeneous domain below the layered medium, we resort to a second scheme.

Scheme 2. *Optimal observation period.*

Accordingly, we seek to optimize the observation period based on (assumed) wave travel times, so that we take into account information stemming only from the layers contained within the finite computational domain, that is, only up to the truncation depth. The process can be summarized as follows: (a) first, we truncate the domain at an arbitrary depth $x=l$. We start with a homogeneous assumption for the target profile, i.e., with $\alpha(x)=\alpha^{(0)}$, and set the observation period $T^{(0)}$ such that

$$T^{(0)} = t_d + 2\frac{l}{\sqrt{\alpha^{(0)}}}, \tag{47}$$

where $\sqrt{\alpha^{(0)}}$ represents velocity, and t_d denotes the duration of the excitation. That is, $T^{(0)}$ is set equal to the duration of the excitation t_d, augmented by twice the travel time it will take for the signal to travel down and up the truncated domain of size l. (b) We then invert for the material profile, and obtain the, in general, inhomogeneous distribution $\alpha^{(1)}(x)$. (c) Next, using the new profile, we update the observation time, as

$$T^{(i)} = t_d + 2\int_0^l \frac{1}{\sqrt{\alpha^{(i)}(x)}}\,\mathrm{d}x, \tag{48}$$

where i denotes the i-th iteration. Steps (b) and (c) are repeated until convergence, where, again, convergence is considered to have been attained when there is small difference between successive profiles.

8. Numerical experiments

We discuss the performance of the described schemes with the aid of numerical experiments. First, we consider reconstructing the sharply varying modulus profile depicted in Fig. 2(a); the target profile is expressed as

$$\alpha(x) = \begin{cases} 1.5, & 0.00 \leqslant x < 0.25, \\ 1.5 + 90(x-0.25), & 0.25 \leqslant x < 0.30, \\ 6.0, & 0.30 \leqslant x < 0.60, \\ 4.0, & 0.60 \leqslant x < 0.90, \\ 7.0, & 0.90 \leqslant x < 1.20, \\ 9.0, & 1.20 \leqslant x < 1.50, \\ 12.0, & 1.50 \leqslant x. \end{cases} \tag{49}$$

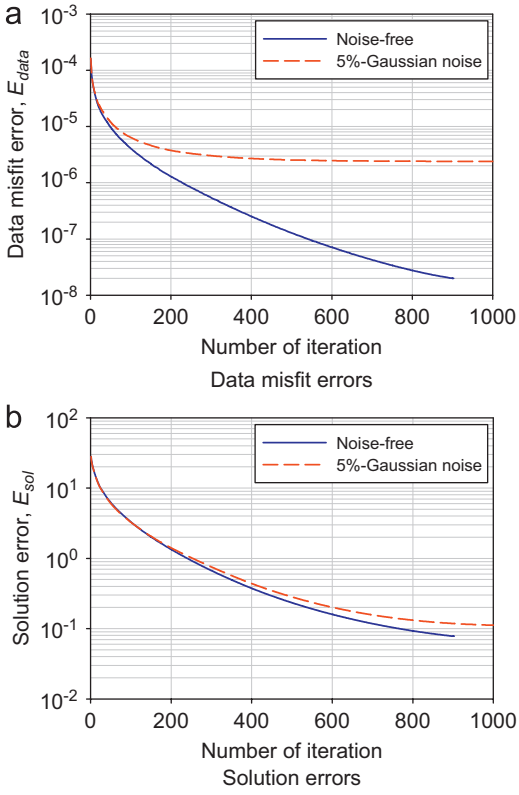

Fig. 6. Data misfit (a) and solution errors (b).

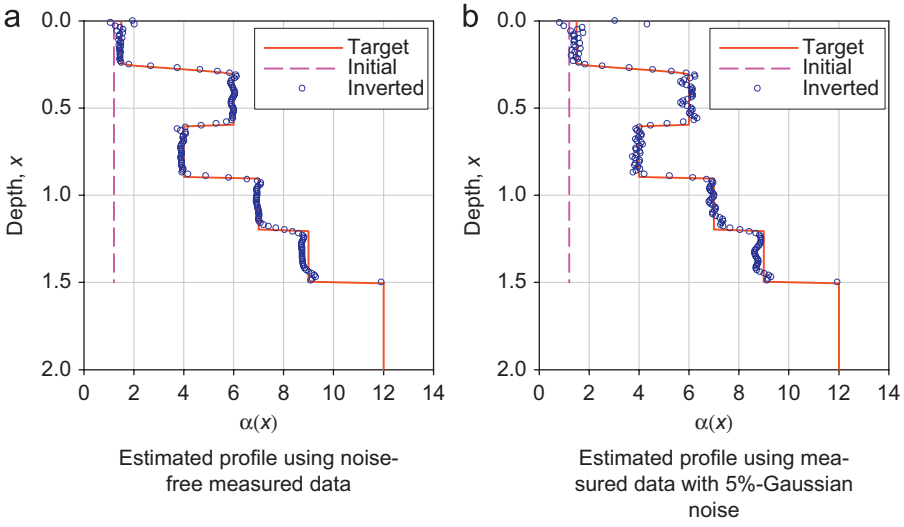

Fig. 5. Target, initial, and estimated profiles of $\alpha(x)$. (a) Estimated profile using noise-free measured data and (b) estimated profile using measured data with 5%-Gaussian noise.

Clearly, beyond $x = 1.5$ and extending to infinity we assume the medium to be homogeneous with $\alpha = 12.0$. First, we truncate the domain at precisely the start of the semi-infinite homogeneous region, as if there were *a priori* knowledge on its precise location, simply to exercise the inversion algorithm under ideal conditions. The initial profile guess is set at $\alpha(x) = 1.2$ (Fig. 2), that is, we assume the entire domain to be homogeneous. The target profile and the initial estimate are depicted in Fig. 2(b). The source excitation is a rapidly decaying pulse-like signal given by (50). Both the signal and its Fourier transform are depicted in Fig. 3:

$$f(t) = \exp\left[-\frac{(t-0.1)^2}{0.0003}\right]. \tag{50}$$

We synthesize the measured data for the given source, and invert for the modulus profile using both noise-free and noisy data. To avoid committing a classic "inverse crime," we use a different mesh when computing the synthetic (measured) data, than the one we use for inversion. More importantly, when computing the

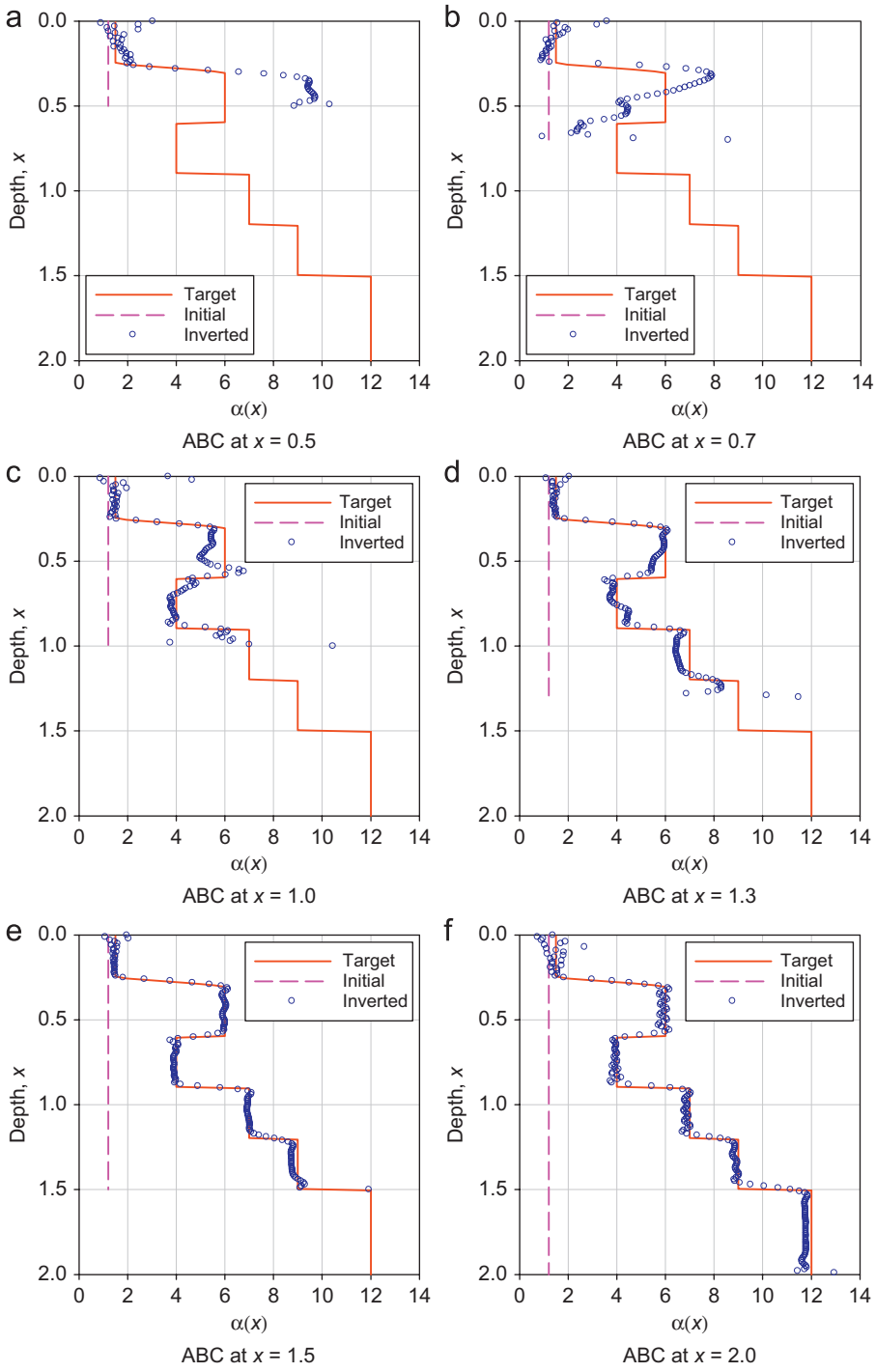

Fig. 7. Target, initial, and estimated profiles of $\alpha(x)$; observation period T is fixed at 3 s. (a) ABC at $x = 0.5$; (b) ABC at $x = 0.7$; (c) ABC at $x = 1.0$; (d) ABC at $x = 1.3$; (e) ABC at $x = 1.5$; (f) ABC at $x = 2.0$.

synthetic data, we use a domain that is considerably larger than the target, so as to guarantee reflection-free synthetic data on the surface. To simulate noise in the data we add Gaussian noise having a standard deviation of 5% with respect to the maximum amplitude of the measured data. The noise-free and noisy data are depicted in Fig. 4. Based on the given measured data, we invert for the modulus profile via Algorithm 1. The results shown in Fig. 5 exhibit quite satisfactory performance for both the noise-free data and noisy data cases. It can also be seen that the profile estimated in (Fig. 5(b)) is a bit more oscillatory due to the presence of noise in the data.

At every iteration, we compute a data misfit error and a solution error norm between the estimated and target profiles; specifically:

$$E_{\text{data}} = \frac{1}{2}\int_0^T [u(0,t) - u_m(0,t)]^2 \, \mathrm{d}t, \tag{51}$$

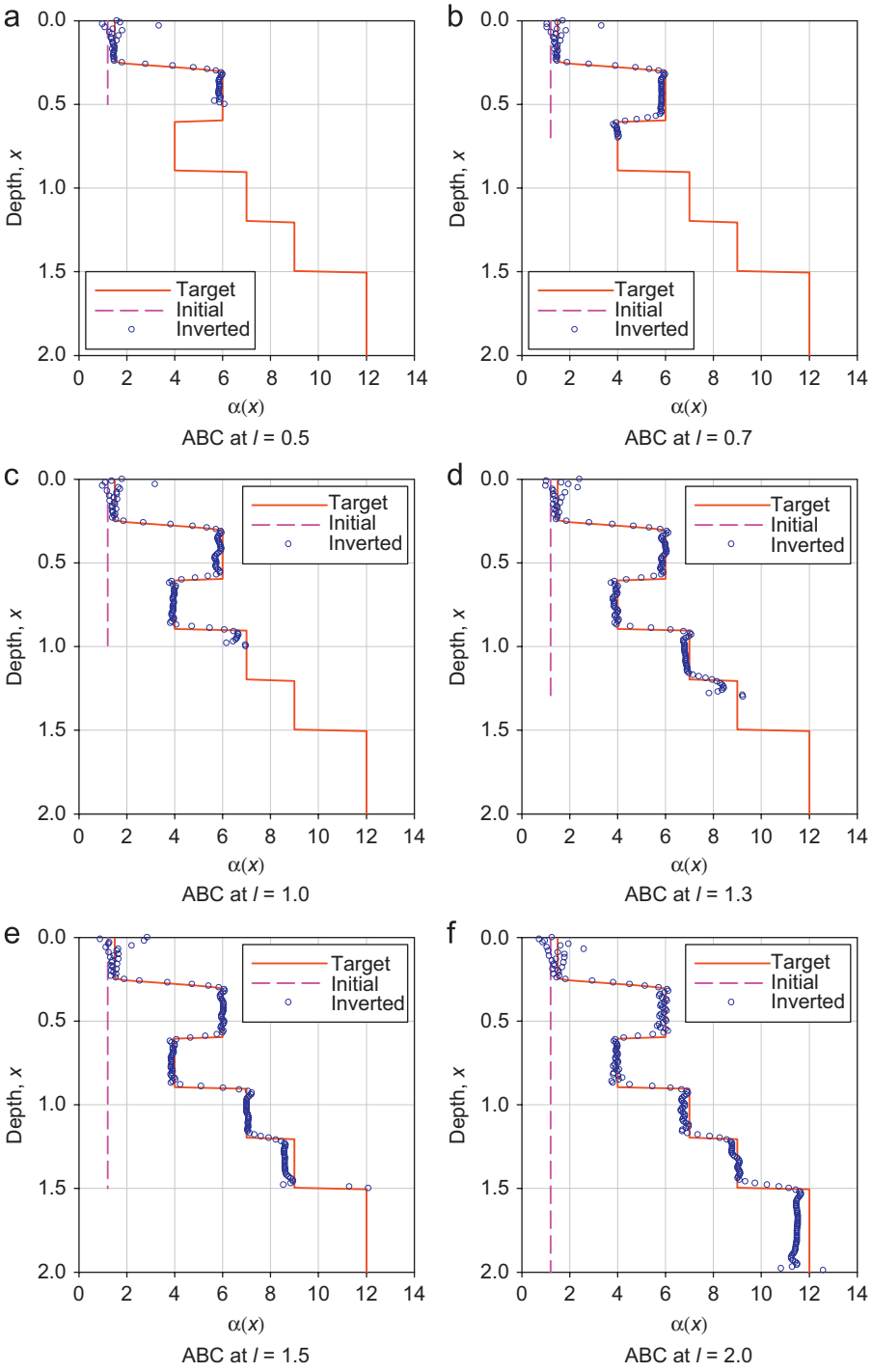

Fig. 8. Target, initial, and estimated profiles of $\alpha(x)$: observation period T is optimized. (a) ABC at $l = 0.5$; (b) ABC at $l = 0.7$; (c) ABC at $l = 1.0$; (d) ABC at $l = 1.3$; (e) ABC at $l = 1.5$; (f) ABC at $l = 2.0$.

$$E_{\text{sol}} = \sum_{i=1}^{N} [\alpha_{\text{exact}}(x_i) - a_i]^2 \Delta x. \quad (52)$$

In the above, E_{data} denotes the data misfit error, which is the misfit functional given in (9) without the regularization term. E_{sol} denotes the solution error, in which Δx is the length of the discrete elements, and x_i is the element midpoint. In Fig. 5 both norms have been plotted for, both, the noise-free and noisy data cases. It can be seen that, as expected, the errors for the noisy data case are higher than the noise-free data case. However, both cases converge quite nicely to the target profile.

Next, we consider the more realistic case where it is not *a priori* known where to best truncate the physical domain. We use again the same sharply varying profile depicted in Fig. 2. To address the problem we used the inversion Algorithm 1 in conjunction with the two iterative Schemes 1 and 2 discussed in the previous section for addressing the truncation boundary difficulty.

First, we fix the observation period T at 3 s, and iteratively increase the domain length l from 0.5 to 2.0, using Scheme 1. As shown in Fig. 6, for the cases of $l = 0.5$, 0.7, and 1.0, there are differences between successive profiles, which imply that the location of the truncation boundary was inappropriate. However, for $x = 1.3$, 1.5, and 2.0, the solutions are quite close to each other, and thus we consider the process converged (could consider even the profile corresponding to truncation depth $x = 1.3$ satisfactory). As it can be seen from Fig. 6 the recovered profiles for the last two cases (e) and (f) agree quite well with the target profile.

Next, we fix the domain size at l. We consider different domain sizes $l = 0.5$, 0.7, 1.0, 1.3, 1.5, and 2.0, and for each one of them we seek to optimize the observation period T based on (48). The reconstructed profiles are shown in Fig. 8. For each one of these cases, the profile has been remarkably well reconstructed up to the considered domain depth. Notice the contrast between, for example, Figs. 7(b) and 8(b), where, for the same truncation depth, the scheme where the observation period is iteratively optimized to match the inverted profile, yields far superior results. In fact, the results in Fig. 8 suggest that the iterative scheme based on the observation period (Scheme 2) yields excellent results regardless of the domain depth l.

9. Conclusions

We discussed a PDE-constrained optimization approach for reconstructing the material profile in a semi-infinite horizontally layered heterogeneous soil medium based on surface measurements of the soil's response to surface excitation. The process is endowed with absorbing boundary conditions to account for the introduction of truncation boundaries, which are necessary when dealing with physical domains of semi-infinite extent. We presented a formal framework for the systematic treatment of such problems under the auspices of a time-dependent regularization scheme, though spatial regularization schemes are equally possible. In addition, to address the cases where there is no homogeneous bottom layer, or its precise location is not *a priori* known, we proposed two iterative schemes based (a) on the iterative relocation of the truncation boundary; or (b) on optimizing the observation period over which we compute solutions to the inversion process. To study the algorithmic performance, we carried out numerical experiments with sharply varying target profiles using both noise-free and noisy data.

Through the results we observed that the time-dependent regularization scheme, thus far used only on fixed-end domains, works quite satisfactorily for semi-infinite domains, even in the presence of absorbing boundary conditions, that typically add noise to the solution (even for forward problems). In addition, it also appears that the observation period iterative scheme that we proposed captures the target profile regardless of the location of the truncation boundary. The overall approach is readily scalable to problems in higher dimensions.

Acknowledgments

Partial support for the authors' research discussed herein has been provided by the National Science Foundation under Grant awards CMS-0348484 and ATM-0325125. This support is gratefully acknowledged.

References

[1] Stokoe KH, Wright SG, Bay JA, Roesset JM. Characterization of geotechnical sites by SASW method. In: Woods RD, editor. Geophysical characterization of sites. New Delhi, India: Oxford & IBH Pub. Co.; 1994. p. 15–25.
[2] Akcelik V. Multiscale Newton–Krylov methods for inverse acoustic wave propagation. Dissertation presented in partial fulfillment of the requirements for the doctoral degree, Carnegie Mellon University, USA, 2002.
[3] Akcelik V, Biros G, Ghattas O. Proceedings of the IEEE/ACM SC2002 conference on parallel multiscale Gauss–Newton–Krylov methods for inverse wave propagation. Baltimore, MD, 2002.
[4] Akcelik V, Bielak J, Biros G, Epanomeritakis I, Ghattas O, Kallivokas LF, Kim EJ. A framework for online inversion-based 3D site characterization. In: Lecture notes in computer science, Computational science—2004, vol. 3038. Berlin: Springer; 2004. p. 717–24.
[5] Lions JL. Optimal control of systems governed by partial differential equations. Berlin, Heidelberg, New York: Springer; 1971.
[6] Chan TF, Tai X-C. Identification of discontinuous coefficients in elliptic problems using total variation regularization. SIAM J Sci Comput 2003; 25(3):881–904.
[7] Akcelik V, Bielak J, Biros G, Epanomeritakis I, Fernandez A, Ghattas O, et al. High-resolution forward and inverse earthquake modeling on terascale computers. In: Proceedings of ACM/IEEE SC2003. Phoenix, AZ, 2003.
[8] Tadi M. Explicit method for inverse wave scattering in solids. Inverse Probl 1997;13(2):509–21.
[9] Tadi M. Evaluation of the elastic property based on boundary measurement. Acta Mech 1998;129(3–4):231–41.
[10] Na S-W, Kallivokas LF. On the inverse problem of soil profile reconstruction—a comparison of time-domain approaches. Comput Mech 2008;42(6): 921–42.
[11] Tikhonov AN. Solution of incorrectly formulated problems and the regularization method. Sov Math Dokl 1963;4:1035–8.
[12] Rudin L, Osher S, Fatemi E. Nonlinear total variation based noise removal algorithms. Physica D 1992;60:259–68.
[13] Barry A, Bielak J, MacCamy RC. On absorbing boundary conditions for wave propagation. J Comput Phys 1988;79:449–68.